

Fermi Observations of High-Energy Gamma-Ray Emission from GRB 080916C

The Fermi LAT and Fermi GBM Collaborations*

Gamma-ray bursts (GRBs) are highly energetic explosions signaling the death of massive stars in distant galaxies. The Gamma-ray Burst Monitor and Large Area Telescope onboard the Fermi Observatory together record GRBs over a broad energy range spanning about 7 decades of gamma-ray energy. In September 2008, Fermi observed the exceptionally luminous GRB 080916C, with the largest apparent energy release yet measured. The high-energy gamma rays are observed to start later and persist longer than the lower energy photons. A simple spectral form fits the entire GRB spectrum, providing strong constraints on emission models. The known distance of the burst enables placing lower limits on the bulk Lorentz factor of the outflow and on the quantum gravity mass.

Gamma-ray bursts (GRBs) are the most luminous explosions in the universe and are leading candidates for the origin of ultrahigh-energy cosmic rays (UHECRs). Prompt emission from GRBs from ~ 10 keV to ~ 1 to

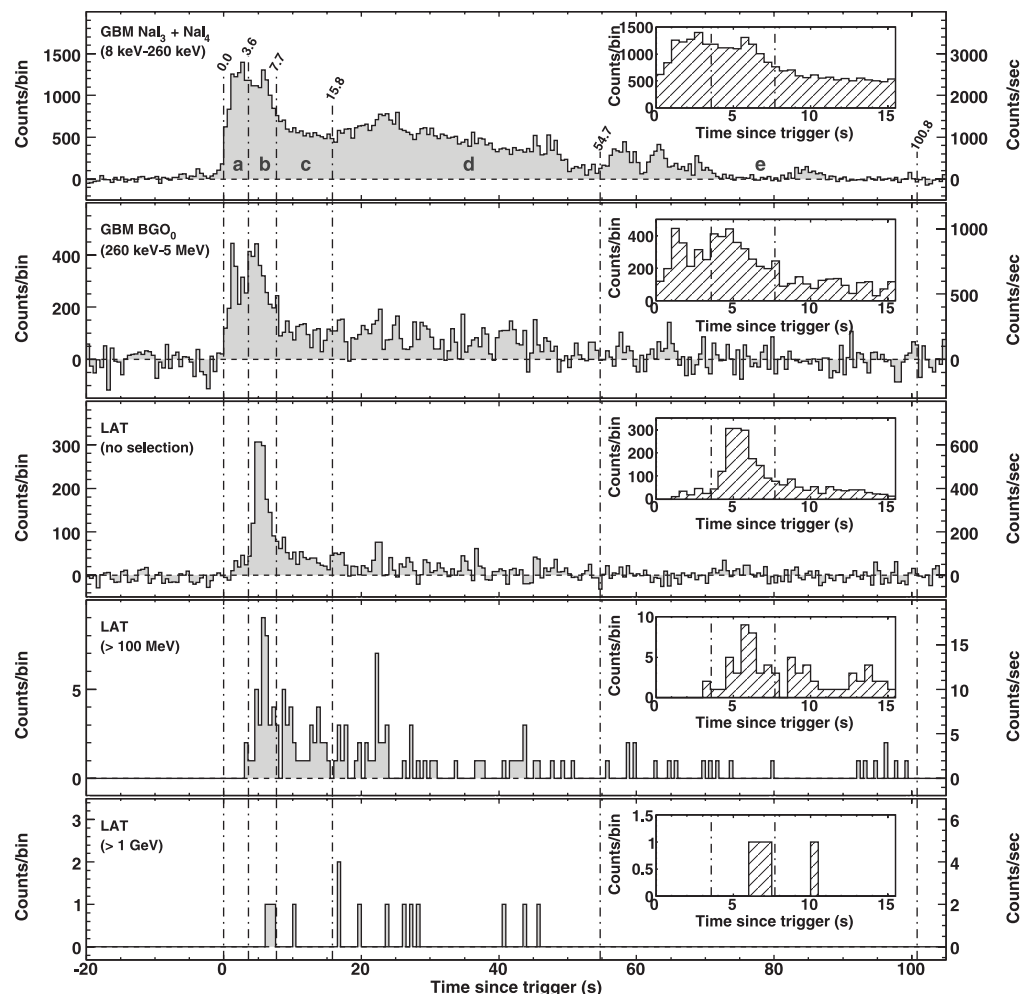
5 MeV has usually been detected, but occasionally photons above 100 MeV have been detected by the Energetic Gamma-Ray Experiment Telescope (EGRET) (1) and more recently by Astro-rivelatore Gamma a Immagini LEggero (AGILE) (2). Observations of gamma rays with energies >100 MeV are particularly prescriptive because they constrain the source environment

and help understand the underlying energy source. Although there have been observations of photons above 100 MeV (3–5), it has not been possible to distinguish competing interpretations of the emission (6–8). The Fermi Gamma-ray Space Telescope, launched on 11 June 2008, provides broad energy coverage and high GRB sensitivities through the Gamma-ray Burst Monitor (GBM) and the Large Area Telescope (LAT) (9). The GBM consists of 12 sodium iodide (NaI) detectors, which cover the energy band between 8 keV and 1 MeV, and two bismuth germanate (BGO) scintillators, which are for the energy band between 150 keV and 40 MeV. The LAT is a pair conversion telescope with the energy coverage from below 20 MeV to more than 300 GeV (supporting online text). In this paper, we report detailed measurements of gamma-ray emission from the GRB 080916C detected by the GBM and LAT.

Observations. At 00:12:45.613542 UT (T_0) on 16 September 2008 the GBM flight software triggered on GRB 080916C. The GRB produced large signals in 9 of the 12 NaI detectors and in one of the two BGO detectors. Analysis of the data on the ground localized the burst to a right ascension (RA) = $08^h07^m12^s$, declination

*The full list of authors and affiliations is presented at the end of this paper.

Fig. 1. Light curves for GRB 080916C observed with the GBM and the LAT, from lowest to highest energies. The energy ranges for the top two graphs are chosen to avoid overlap. The top three graphs represent the background-subtracted light curves for the NaI, the BGO, and the LAT. The top graph shows the sum of the counts, in the 8- to 260-keV energy band, of two NaI detectors (3 and 4). The second is the corresponding plot for BGO detector 0, between 260 keV and 5 MeV. The third shows all LAT events passing the onboard event filter for gamma-rays. (Insets) Views of the first 15 s from the trigger time. In all cases, the bin width is 0.5 s; the per-second counting rate is reported on the right for convenience.



(Dec.) = $-61^{\circ}18'00''$ (10), with an uncertainty of 2.8° at 68% confidence level (C.L.).

At the time of the trigger, the GRB was located $\sim 48^{\circ}$ from the LAT boresight, and on-ground analysis revealed a bright source consistent with the GRB location. Using the events collected during the first 66 s after T_0 , within 20° around the GBM burst position, the LAT provided a localization of RA = $07^{\text{h}}59^{\text{m}}31^{\text{s}}$, Dec. = $-56^{\circ}35'24''$ (11) with a statistical uncertainty of 0.09° at 68% C.L. (0.13° at 90% C.L.) and a systematic uncertainty smaller than $\sim 0.1^{\circ}$ (movie S1).

Follow-up x-ray and optical observations revealed a fading source at RA = $07^{\text{h}}59^{\text{m}}23.24^{\text{s}}$, Dec. = $-56^{\circ}38'16.8''$ ($\pm 1.9''$ at 90% C.L.) (12) by Swift/X-Ray Telescope (XRT) and RA = $07^{\text{h}}59^{\text{m}}23.32^{\text{s}}$, Dec. = $-56^{\circ}38'18.0''$ ($\pm 0.5''$) (13, 14) by Gamma-Ray Burst Optical/Near-Infrared Detector (GROND), respectively, consistent with the LAT localization within the estimated uncertainties. GROND determined the redshift of this source to be $z = 4.35 \pm 0.15$ (15). The afterglow was also observed in the near-infrared band by the Nagoya-SAAO 1.4 m telescope (IRSF) (16). The x-ray light curve of the afterglow from $T_0 + 61$ ks to $T_0 + 1306$ ks shows two temporal breaks at about 2 and 4 days after the trigger (17). The light curves before, between, and after the breaks can be fit with a power-law function with decay indices ~ -2.3 , ~ -0.2 , and ~ -1.4 , respectively.

The light curve of GRB 080916C, as observed with Fermi GBM and LAT, is shown in Fig. 1. The total number of LAT counts after background subtraction in the first 100 s after the trigger was >3000 . For most of the low-energy events, however, extracting reliable directional and energy information was not possible. After we applied standard selection cuts (9) for transient sources with energies greater than 100 MeV and directions compatible with the burst location, 145 events remained (panel 4), and 14 events had energies > 1 GeV (panel 5).

Because of the energy-dependent temporal structure of the light curve, we divided the light curve into five time intervals (a, b, c, d, and e) delineated by the vertical lines (Fig. 1). The GRB light curve at low energy has two bright peaks, one between 0 and 3.6 s after the trigger (interval a) and one between 3.6 and 7.7 s (interval b). The two peaks are distinct in the BGO light curve but less so in the NaI. In the LAT detector the first peak is not significant though the light curve shows evidence of activity in time interval a, mostly in events below 100 MeV. Above 100 MeV, peak b is prominent in the LAT light curve. Interval c coincides with the tail of the main pulse, and the last two intervals reflect temporal structure in the NaI light curve and have been chosen to provide enough statistics in the LAT energy band for spectral analysis. The highest energy photon was observed during interval d: $E_{\text{h}} = 13.22^{+0.70}_{-1.54}$ GeV. Most of the emission in peak b shifts toward later times as the energy increases (inset).

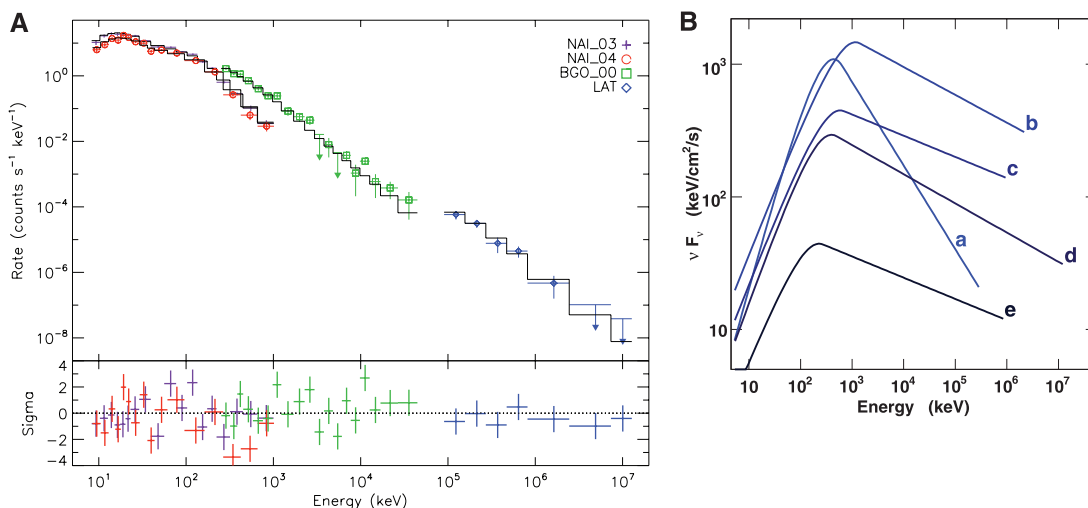
Spectral analysis. We performed simultaneous spectral fits of the GBM and LAT data for each of the five time bins described above and shown in Fig. 1 (see Fig. 2 for an example of the fits). GBM NaI data from detectors 3 and 4 were selected from 8 keV to 1.0 MeV, as well as BGO detector 0 data from 0.26 to 40 MeV. LAT photons were selected by using the “transient” event class (9) for the energies from 100 MeV to 200 GeV. This event class provides the largest effective area and highest background rates among the LAT standard event classes, which is appropriate for bright sources with small backgrounds like this burst. This combination of the GBM and LAT data results in joint spectral fits by using forward-folding techniques covering over 7 decades of energy [supporting online material (SOM) text].

The spectra of all five time intervals are well fit by the empirical Band function (18), which smoothly joins low- and high-energy power laws. The first time interval, with a relative paucity of

photons in the LAT, also has the most distinct spectral parameter values. The low-energy photon index α is larger (indicating harder emission), and the high-energy photon index β is smaller (indicating softer emission), consistent with the small number of LAT photons observed at this time. After the first interval there was no significant evolution in either α or β , as is evident in Fig. 3. In contrast, E_{peak} , the energy at which the energy emission peaks in the sense of energy per photon energy decade, evolved from the first time bin to reach its highest value in the second time bin, then softened through the remainder of the GRB. The higher E_{peak} and overall intensity of interval b, combined with the hard value of β that is characteristic of the later intervals, are the spectral characteristics that lead to the emission peaking in the LAT light curve (Fig. 1). The spectrum of interval b with a Band function fit is shown in Fig. 2. Comparing the parameters of this interval to the ensemble of EGRET burst detections, we find that the flux at around 1 MeV and β are similar to those for GRB 910503 and that E_{peak} resembles that for GRB 910814 (19).

We searched for deviations from the Band function, such as an additional component at high energies (5). Three photons in the fourth time bin had energies above 6 GeV. We tried modeling these high-energy photons with a power law as an additional high-energy spectral component. Compared to the null hypothesis that the data originated from a simple Band GRB function, adding the additional power-law component resulted in a probability of 1% that there was no additional spectral component for this time bin; with five time bins, this is not strong evidence for any additional component. Our sensitivity to higher-energy photons may be reduced at $z \sim 4.35$ through absorption by extragalactic background light (EBL). Because the effect of various EBL models ranges widely, from leaving the single time bin spectral-fit probability of an extra component unchanged (20) to decreasing the

Fig. 2. (A) Count spectrum for NaI, BGO, and LAT in time bin b: The data points have 1σ error bars, whereas upper limits are 2σ . The histograms show the number of counts obtained by folding the photon model through the instrument response models. Spectra for time intervals a to e over the entire energy fit range are available in figs. S1 to S5. **(B)** The model spectra in νF_{ν} units for all five time intervals, in which a flat spectrum would indicate equal energy per decade of photon energy, and the changing shapes show the evolution of the spectrum over time. The curves end at the energy of the highest-energy photon observed in each time interval.



spectral-fit plausibility of its absence to 0.03% (21), we cannot use EBL absorption effects in our estimation of significance.

Long-lived emissions. Although the light curves shown in Fig. 1 indicate that during interval e the spiky structures typical of prompt GRB emission appear to be dying out, the emission persisted in some of the GBM NaI detectors at a low level out to nearly $T_0 + 200$ s. The lack of pulse structure and the background-limited nature of the NaI detectors make this emission difficult to associate conclusively with the GRB, but the excess above background in the 12 NaI detectors occurred in the ratios expected for the geometry of the detectors relative to the burst direction. In addition, this type of low-level, extended emission is a known phenomenon in at least some long GRBs (22), so we associate it with the GRB and fit the spectrum with a power-law index of -1.92 ± 0.21 (1σ uncertainty). Emission beyond $T_0 + 200$ s fell below the threshold of the GBM detectors. Because of much lower instrumental backgrounds in the LAT, a high-energy decaying component might be seen for a longer time. The most suitable class to study faint sources with minimum backgrounds (“diffuse”) was used to select events within 15° of the GROND localization coordinates between $T_0 + 100$ s and $T_0 + 1400$ s, which were then examined for possible connection with the GRB source. The interval up to $T_0 + 200$ s was treated separately for correlation with contemporaneous data from the GBM. The upper bound was chosen because, after $T_0 + 1400$ s, the GRB off-axis angle increased from 50° to 62° , resulting in decreased effective area.

We performed unbinned maximum likelihood fits of a power-law spectral function for a point source at the GROND-determined burst location in these two time intervals. Contributions from instrumental, Galactic, and extragalactic components were included in the fit, as well as the bright source Vela (which is located 13° from the GRB). Both time intervals show the presence of significant flux. For the final time interval, $T_0 + 200$ to $T_0 + 1400$ s, the fit yields a flux of $(6.4 \pm 2.5) \times 10^{-6} \text{ } \gamma \text{ cm}^{-2} \text{ s}^{-1}$ for $E > 100$ MeV with a power-law photon index of -2.8 ± 0.5 at a significance of 5.6σ . The fitting process does not assign individual photons to particular sources; it predicts, however, that 10.4 of the fitted photons originated from the GRB. If the position of the point source is left free instead of fixed to the GROND localization, the fit yields a source position of $RA = 07^h57^m33^s$, $Dec. = -57^\circ00'00''$ with an uncertainty of 0.51° at 90% C.L. This location is 0.45° from, and in agreement with, the GROND GRB position. To solidify the association of this extended emission with the GRB, we performed the same source detection procedure for data from $T_0 - 900$ s to T_0 , and no emission was observed. A search for emission beyond $T_0 + 1400$ s was also fruitless.

We therefore associate this long-lived component with the GRB and include it as a sixth and

a seventh time interval for comparison with the early-time emission (Fig. 4). In the LAT data, a constantly declining high-energy flux with a power-law decay index of -1.2 ± 0.2 is seen throughout $T_0 + 1400$ s (red points, Fig. 4). On the other hand, the flux in the GBM band shows a slower decay initially and an apparent break in the light curve at $\sim T_0 + 55$ s. The power-law decay indices are about -0.6 and -3.3 before and after the break, respectively. Previous reports (3, 5) have provided tantalizing clues that distinct high-energy components may be a feature of some GRBs.

Interpretation. The Fermi observations of GRB 080916C show that the event energy spectra up to ~ 100 s are consistent with a single model (Band function), suggesting that a single emission mechanism dominates.

Between 10 keV and 10 GeV in the observer's frame, we measure a fluence $f = 2.4 \times 10^{-4} \text{ ergs cm}^{-2}$, which gives at $z = 4.35$ an apparent isotropic energy release for a standard cold dark

matter cosmology with cosmological constant $\Omega_\Lambda = 0.73$, $\Omega_m = 0.27$, and a Hubble's constant of $71 \text{ km s}^{-1} \text{ Mpc}^{-1}$ of $E_{\text{iso}} \cong 8.8 \times 10^{54} \text{ ergs}$ (SOM text). This is ~ 4.9 times the Solar rest energy and therefore strongly suggests on energetic grounds, for any stellar mass progenitor, that the GRB outflow powering this emission occupied only a small fraction ($\leq 10^{-2}$) of the total solid angle and was collimated into a narrow jet. A comparison with the previous highest measured $E_{\text{iso}} = 2.0 \times 10^{54}$ from 20 keV to 2 MeV shows the fluence and E_{iso} for GRB 080916C in this energy range are $1.2 \times 10^{-4} \text{ ergs cm}^{-2}$ and $4.3 \times 10^{54} \text{ ergs}$, respectively. This earlier burst, GRB 990123 (23), was detected up to ~ 20 MeV by the EGRET Total Absorption Shower Counter instrument.

High-energy γ rays from such intense regions can be strongly attenuated by lower-energy photons via pair production. The pair-production opacity can be reduced if the emission region is moving toward us at highly relativistic speeds—a

Fig. 3. Fit parameters for the Band function, α , β , and E_{peak} as a function of time. Error bars indicate 1σ uncertainty.

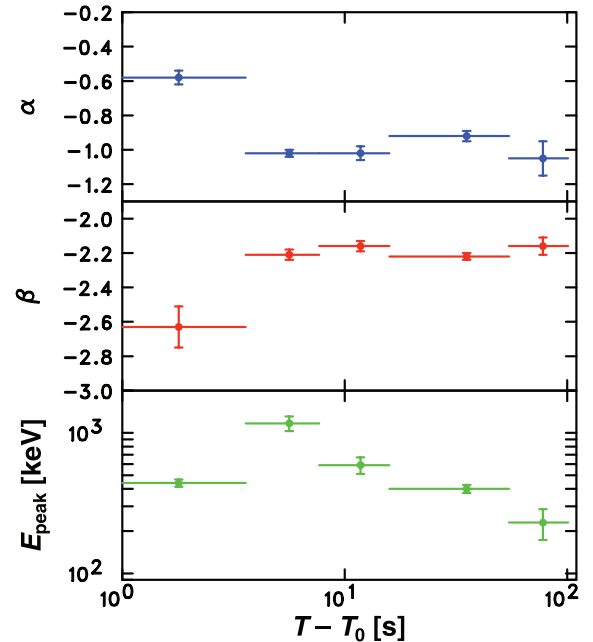
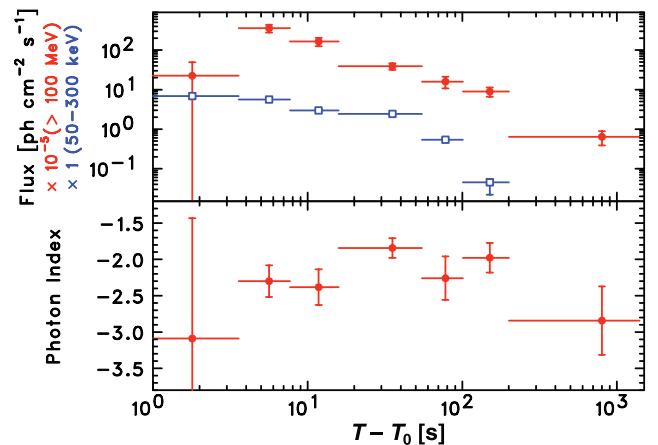


Fig. 4. Fluxes (top) for the energy ranges 50 to 300 keV (shown in blue open squares) and above 100 MeV (red solid squares) and power-law index as a function of the time from T_0 to $T_0 + 1400$ s [(bottom) LAT data only]. The red points are obtained by spectral fits of the LAT-only data for all time intervals. The blue points are obtained with the Band functions listed in Table 1 for the first five intervals and a power-law fit with index -1.90 ± 0.05 for the sixth interval.



relativistic jet with Lorentz factor Γ also explains the intensity and rapid variability of GRB γ rays (24–28). The observed correlated variability of the GBM and LAT emissions indicates that photons formed co-spatially, with the lower-energy (GBM) photons providing target photons that can interact with higher energy γ rays to produce electron-positron pairs. By using the Band function as the target radiation field and setting to unity the optical depth $\tau_{\gamma\gamma}$ to γ -ray pair production attenuation of the highest-energy observed photon, we calculate Γ_{\min} , the minimum bulk Lorentz factor (supporting online text) (Fig. 5). For $z = 4.35$, we obtain $\Gamma_{\min} = 608 \pm 15$ and 887 ± 21 in time bins d and b, respectively. For a spherical emitting shell of radius R , the observed variability time Δt and Γ_{\min} can be used to set a lower limit on the emission radius, $R > \Gamma_{\min}^2 c \Delta t / (1+z) = 8.9 \times 10^{15} (\Gamma_{\min}/890)^2 (\Delta t/2 \text{ s}) [5.35/(1+z)] \text{ cm}$. Similarly large prompt emission radii were inferred for other GRBs on different grounds (29, 30).

The delayed onset of the GRB 080916C LAT pulse, which coincides with the rise of the second peak in the GBM light curve (Fig. 1), suggests a common origin in a region spatially distinct from the first GBM pulse. In the framework of the internal-shocks model for the prompt emission of

GRBs (27, 28), where intermittent winds of relativistic plasma are ejected by a newly formed black hole and collide to form shocks and accelerate particles, the two emission regions could arise from two different pairs of colliding shells, with variations in physical conditions leading to nonthermal electrons with different spectral hardnesses.

An alternative explanation for the delayed onset of the LAT emission is that a volume becomes filled with radiation that attenuates the high-energy photons until a later time when the emitting region expands and becomes optically thin. A $\gamma\gamma$ pair-production opacity effect would, however, produce a high-energy spectral softening or cutoff, whereas in all cases the combined GBM/LAT data are well fit with simple models by using the Band parameterization. Moreover, internal γ -ray opacity models predict that high-energy photons should also be detected in the rising portion of the GBM emission while they can still escape the source, before the increased photon density attenuates the γ rays (31). Lastly, in hadronic models associated with UHECR and high-energy neutrino production, the delay of the LAT emission could be a consequence of the time needed to accelerate protons or ions to energies

where they can radiate by photopion or proton synchrotron radiation and generate an electromagnetic cascade (32–34). It is, however, unclear whether such models can reproduce the observed 10-keV to 10-GeV spectrum.

Before our observations, a high-energy ($\geq 100 \text{ MeV}$) tail was observed most clearly from GRB 940217 (3) in observations by EGRET. The continuous high-energy tail in GRB 080916C could be due to the delayed arrival of the SSC emission in the GeV energy band during the afterglow phase (35). The observations, however, lack the predicted spectral hardening expected as the GeV emission changes from prompt synchrotron to afterglow SSC radiation. The LAT high-energy tail could also result from angle-dependent scattering effects (36) or from cascades induced by ultrarelativistic ions accelerated in GRBs (8).

The lack of two distinct emission components in the spectra up to $\sim 10 \text{ GeV}$ throughout the burst is compatible with a nonthermal synchrotron origin of the radiation. This is the favored emission mechanism at keV to MeV energies (27) and can indeed reach $\sim 30(\Gamma/1000)[5.35/(1+z)] \text{ GeV}$ (37). Nonthermal synchrotron radiation should, however, be accompanied by a synchrotron self-Compton (SSC) spectral component produced from electrons that Compton upscatter their synchrotron photons to gamma-ray energies potentially in the LAT energy band. The apparent lack of an SSC component indicates that the magnetic energy density is much higher than the electron energy density (SOM text) or that the SSC νF_{ν} spectrum peaks at $\gg 10 \text{ GeV}$ and thus cannot be detected, which requires a typical electron Lorentz factor $\gamma_m \sim (E_{\text{peak}}^{\text{SSC}}/E_{\text{peak}}^{\text{syn}})^{1/2} \gg 100$.

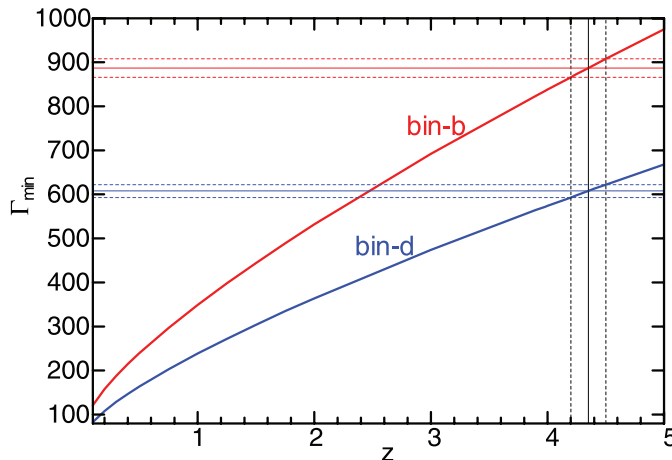
In addition to these considerations, sensitivity to a high-energy additional spectral component is reduced because EBL can absorb high-energy photons via pair-production interactions. In GRB 080916C, we did not observe a spectral cutoff that might be a signature of EBL, nor does the observation of a 13.2-GeV photon discriminate between EBL models (SOM text). However, if EBL is hiding an additional spectral component, we may be underestimating the energetics of GRB 080916C.

The high photon energies and large distance of GRB 080916C can test a prediction of some quantum gravity models that energy dispersion exists in the speed of photons, high-energy photons traveling slower and therefore arriving to us later than low-energy photons (38). In the linear approximation, the difference in the arrival times Δt is proportional to the ratio of photon energy difference to the quantum gravity mass, $\Delta E/M_{\text{QG}}$, and depends on the distance the photons traveled. The arrival time of the $13.2_{-1.54}^{+0.70} \text{ GeV}$ photon relative to T_0 , $t = 16.54 \text{ s}$, is a conservative upper limit on its Δt relative to $\sim \text{MeV}$ photons and implies a robust lower limit on the quantum gravity mass, $M_{\text{QG}} > 1.3 \times 10^{18} \text{ GeV}/c^2$ (SOM text). We have used the low-end of the 1σ confidence intervals of both z and E_h in cal-

Table 1. Fit parameters for the Band function A , α , β , and E_{peak} as a function of time. Uncertainties are statistical in nature; the maximum possible systematic errors on the parameter values are comparable to their statistical errors (SOM text). Times are relative to trigger time $T_0 = 00:12:45.613542 \text{ UT}$.

Time bin and range (s)	A ($\gamma \text{ cm}^{-2} \text{ s}^{-1} \text{ keV}^{-1}$)	α	β	E_{peak} (keV)	Flux	
					50 to 300 keV ($\gamma \text{ cm}^{-2} \text{ s}^{-1}$)	100 MeV to 10 GeV ($\gamma \text{ cm}^{-2} \text{ s}^{-1}$)
a: 0.004 to 3.58	$(55 \pm 2) \times 10^{-3}$	-0.58 ± 0.04	-2.63 ± 0.12	440 ± 27	6.87 ± 0.12	$(2.5 \pm 1.6) \times 10^{-4}$
b: 3.58 to 7.68	$(35 \pm 1) \times 10^{-3}$	-1.02 ± 0.02	-2.21 ± 0.03	1170 ± 140	5.63 ± 0.09	$(4.8 \pm 0.6) \times 10^{-3}$
c: 7.68 to 15.87	$(21 \pm 1) \times 10^{-3}$	-1.02 ± 0.04	-2.16 ± 0.03	590 ± 80	2.98 ± 0.06	$(1.7 \pm 0.2) \times 10^{-3}$
d: 15.87 to 54.78	$(19.4 \pm 0.7) \times 10^{-3}$	-0.92 ± 0.03	-2.22 ± 0.02	400 ± 26	2.44 ± 0.03	$(7.1 \pm 0.9) \times 10^{-4}$
e: 54.78 to 100.86	$(5.2 \pm 0.9) \times 10^{-3}$	-1.05 ± 0.10	-2.16 ± 0.05	230 ± 57	0.54 ± 0.02	$(1.5 \pm 0.4) \times 10^{-4}$

Fig. 5. The minimum Lorentz factor Γ_{\min} as a function of redshift z for two different pulses in the γ -ray light curve. The value of Γ_{\min} , defined by the condition that the γ -ray absorption opacity $\tau_{\gamma\gamma} = 1$, is derived for 3 GeV and 13 GeV photons and variability time scales $\Delta t = 2.0 \text{ s}$ and 20 s in time bins b and d, respectively.



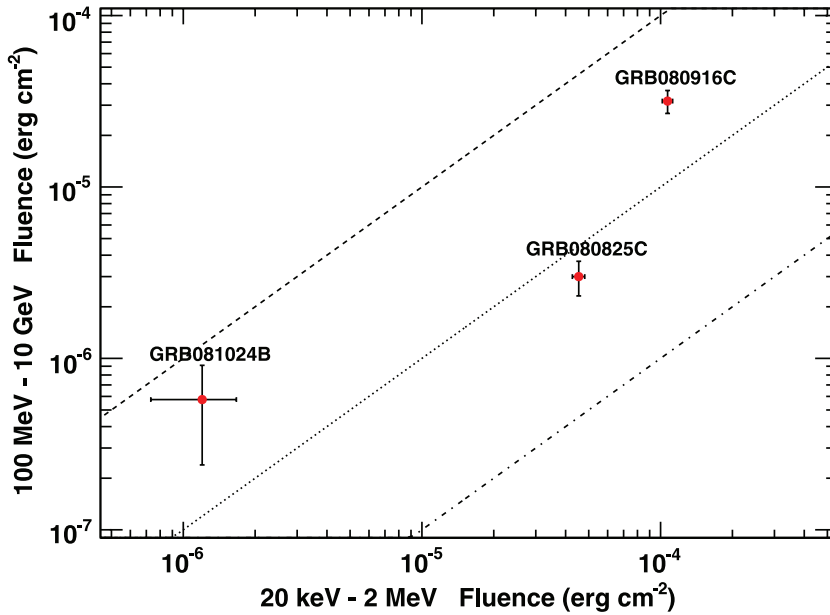


Fig. 6. Low- and high-energy gamma-ray fluences of three GRBs observed with both Fermi instruments. Both energy ranges are two decades. The diagonal lines indicate constant ratios between the two fluences: dashed, LAT and GBM fluences are equal; dotted, LAT fluence is 10% of GBM fluence; dot-dash, LAT fluence is 1% of GBM fluence.

culating M_{QG} . This lower limit is only one order of magnitude smaller than the Planck mass, $1.22 \times 10^{19} \text{ GeV}/c^2$.

In the first 5 months since triggering was enabled on 14 July 2008, GBM triggered on 58 GRBs within the LAT field of view: Besides GRB 080916C (discussed here), two additional events were also seen with the LAT. The first was GRB 080825C (39), and the third was GRB 081024B, the first short GRB observed with the LAT (40, 41). Figure 6 shows the LAT (100 MeV to 10 GeV) versus the GBM (20 keV to 2 MeV) fluences measured during the entire duration of each event. GRB 080916C stands out in both instruments, enabling better statistics in its spectral and timing analyses. Moreover, unlike the other two events, GRB 080916C has a redshift measurement, enabling determinations of lower limits for the bulk Lorentz factor of its ejecta and of the quantum gravity mass M_{QG} .

Figure 6 raises questions about the relation between the low and high energy emission. In no case have we detected a high-energy excess that would imply a distinct spectral component such as an SSC peak. The constraints are, however, weaker for GRBs 081024B and 080825C, which have fewer detected counts with which we could fit additional components. We observe in all three GRBs a delay in the onset of the LAT ($E > 100 \text{ MeV}$) photons with respect to the lower energy GBM photons. This trend is an important clue for unraveling the GRB phenomenon.

References and Notes

1. B. L. Dingus, *Astrophys. Space Sci.* **231**, 187 (1995).
2. A. Giuliani et al., *Astron. Astrophys.* in press; preprint available online at <http://arxiv.org/abs/0809.1230> (2008).
3. K. Hurley et al., *Nature* **372**, 652 (1994).

4. D. N. Wren, D. L. Bertsch, S. Ritz, *Astrophys. J.* **574**, L47 (2002).
5. M. M. González et al., *Nature* **424**, 749 (2003).
6. J. Granot, D. Guetta, *Astrophys. J.* **598**, L11 (2003).
7. J. Katz, *Astrophys. J.* **432**, L27 (1994).
8. C. D. Dermer, A. Atoyan, *New J. Phys.* **8**, 122 (2006).
9. W. B. Atwood et al., <http://arxiv.org/abs/0902.1089> (2008).
10. A. Goldstein, A. vander Horst, *GCN Circ.* **8245** (2008).
11. H. Tajima et al., *GCN Circ.* **8246** (2008).
12. M. Perri et al., *GCN Circ.* **8261** (2008).
13. C. Clemens et al., *GCN Circ.* **8257** (2008).
14. C. Clemens et al., *GCN Circ.* **8272** (2008).
15. J. Greiner et al., <http://arxiv.org/abs/0902.0761> (2009).
16. T. Nagayama et al., *GCN Circ.* **8274** (2008).
17. G. Stratta et al., *GCN Rep.* **166.1** (2008).
18. D. Band et al., *Astrophys. J.* **413**, 281 (1993).
19. M. Baring, *Astrophys. J.* **650**, 1004 (2006).
20. S. Razzaque, C. D. Dermer, J. F. Finke, *Astrophys. J.*, in press; preprint available at <http://arxiv.org/abs/0807.4294> (2008).
21. F. W. Stecker, M. A. Malkan, S. T. Scully, *Astrophys. J.* **648**, 774 (2006).
22. V. Connaughton, *Astrophys. J.* **567**, 1028 (2002).
23. M. S. Briggs et al., *Astrophys. J.* **524**, 82 (1999).
24. J. H. Krolik, E. A. Pier, *Astrophys. J.* **373**, 277 (1991).
25. E. E. Fenimore, R. I. Epstein, C. Ho, *Astron. Astrophys. Suppl. Ser.* **97**, 59 (1993).
26. V. Lithwick, R. Sari, *Astrophys. J.* **555**, 540 (2001).
27. P. Mészáros, *Annu. Rev. Astron. Astrophys.* **40**, 137 (2002).
28. T. Piran, *Phys. Rep.* **314**, 575 (1999).
29. P. Kumar et al., *Mon. Not. R. Astron. Soc.* **376**, L57 (2007).
30. J. L. Racusin, *Nature* **455**, 183 (2008).
31. J. Granot, J. Cohen-Tanugi, E. do Couto e Silva, *Astrophys. J.* **677**, 92 (2008).
32. J. P. Rachen, P. Mészáros, *Phys. Rev. D* **58**, 123005 (1998).
33. C. D. Dermer, *Astrophys. J.* **574**, 65 (2002).
34. S. Razzaque, P. Mészáros, E. Waxman, *Mod. Phys. Lett. A* **20**, 2351 (2005).
35. R. Sari, A. A. Esin, *Astrophys. J.* **548**, 787 (2001).
36. X. Y. Wang, Z. Li, P. Mészáros, *Astrophys. J.* **641**, L89 (2006).
37. A. A. Pe'er, E. Waxman, *Astrophys. J.* **613**, 448 (2004).
38. G. Amelino-Camelia et al., *Nature* **393**, 763 (1998).
39. A. Bouvier et al., *GCN Circ.* **8183** (2008).
40. N. Omodei, *GCN Circ.* **8407** (2008).
41. V. Connaughton, M. S. Briggs, *GCN Circ.* **8408** (2008).

42. A. A. Abdo, J. Finke, and S. Razzaque are National Research Council Research Associates. A. J. van der Horst is a NASA Postdoctoral Program Fellow. The Fermi LAT Collaboration acknowledges the support of a number of agencies and institutes. These include NASA and the Department of Energy in the United States; the Commissariat à l'Energie Atomique and the Centre National de la Recherche Scientifique/Institut National de Physique Nucléaire et de Physique des Particules in France; the Agenzia Spaziale Italiana and the Istituto Nazionale di Fisica Nucleare in Italy; the Ministry of Education, Culture, Sports, Science and Technology (MEXT), High Energy Accelerator Research Organization (KEK), and Japan Aerospace Exploration Agency (JAXA) in Japan; and the K. A. Wallenberg Foundation, the Swedish Research Council, and the Swedish National Space Board in Sweden. J.C. is a Royal Swedish Academy of Sciences Research fellow supported by a grant from the K. A. Wallenberg foundation. The Fermi GBM Collaboration acknowledges the support of NASA in the United States and Deutsches Zentrum für Luft- und Raumfahrt in Germany and thanks L. Gibby, A. English, and F. Kroeger.

***List of authors and affiliations:** A. A. Abdo,¹ M. Ackermann,² M. Arimoto,³ K. Asano,³ W. B. Atwood,⁴ M. Axelsson,^{5,6} L. Baldini,⁷ J. Ballet,⁸ D. L. Band,^{9,10} G. Barbiellini,^{11,12} M. G. Baring,¹³ D. Bastieri,^{14,15} M. Battelino,^{5,16} B. M. Baughman,¹⁸ K. Bechtol,³ F. Bellardi,⁸ R. Bellazzini,⁸ B. Berenji,³ P. N. Bhat,¹⁸ E. Bissaldi,¹⁹ R. D. Blandford,² E. D. Bloom,² G. Bogaert,²⁰ J. R. Bogart,² E. Bonamente,^{21,22} J. Bonnell,¹⁰ A. W. Borgland,² A. Bouvier,² J. Bregeon,⁷ A. Brez,⁷ M. S. Briggs,^{18*} M. Brigida,^{23,24} P. Bruel,²⁰ T. H. Burnett,²⁵ D. Burrows,²⁶ G. Busetto,^{14,15} G. A. Calciandro,^{23,24} R. A. Cameron,² P. A. Caraveo,²⁷ J. M. Casandjian,⁸ M. Ceccanti,⁷ C. Cecchi,^{21,22} A. Celotti,²⁸ E. Charles,² A. Chekhtman,^{1,29} C. C. Cheung,¹⁰ J. Chiang,³¹ S. Ciprini,^{21,22} R. Claus,² J. Cohen-Tanugi,³⁰ L. R. Cominsky,³¹ V. Connaughton,¹⁸ J. Conrad,^{5,16,32} L. Costamante,² S. Cutini,³³ M. DeKlotz,³⁴ C. D. Dermer,^{1*} A. de Angelis,³⁵ F. de Palma,^{23,24} S. W. Digel,² B. L. Dingus,³⁶ E. do Couto e Silva,² P. S. Drell,² R. Dubois,² D. Dumora,^{37,38} Y. Edmonds,² P. A. Evans,³⁹ D. Fabiani,⁷ C. Farnier,³⁰ C. Favuzzi,^{23,24} J. Finke,³ G. Fishman,⁴⁰ W. B. Focke,² M. Fraioli,³⁵ Y. Fukazawa,⁴¹ S. Funk,² P. Fusco,^{23,24} F. Gargano,²⁴ D. Gasparri,³³ N. Gehrels,^{10,42} S. Germani,^{21,22} B. Giebels,²⁰ N. Giuglietto,^{23,24} P. Giommi,³³ F. Giordano,^{23,24} T. Glanzman,² G. Godfrey,² A. Goldstein,¹⁸ J. Granot,⁴³ J. Greiner,¹⁹ I. A. Grenier,⁸ M.-H. Grondin,^{37,38} J. E. Grove,¹ L. Guillemot,^{37,38} S. Guirrec,³⁰ G. Haller,² Y. Hanabata,⁴¹ A. K. Harding,¹⁰ M. Hayashida,² E. Hays,¹⁰ J. A. Hernandez Morata,⁴⁴ A. Hoover,³⁶ R. E. Hughes,¹⁷ G. Jóhannesson,² A. S. Johnson,² R. P. Johnson,⁴ T. J. Johnson,^{10,42} W. N. Johnson,¹ T. Kamae,² H. Katagiri,⁴¹ J. Kataoka,³ A. Kavelaars,² N. Kawai,^{3,45} H. Kelly,² J. Kennea,²⁶ M. Kerr,²⁵ R. M. Kippen,³⁶ J. Knödlseder,⁴⁶ D. Kocevski,² M. L. Kocian,² N. Komin,^{8,30} C. Kouveliotou,⁴⁰ F. Kuehn,¹⁷ M. Kuss,⁷ J. Lande,² D. Landriu,⁸ S. Larsson,^{5,32} L. Latronico,⁷ C. D. Lavalley,³⁰ B. Lee,⁴⁷ S.-H. Lee,² M. Lemoine-Goumard,^{37,38} G. G. Lichti,¹⁹ F. Longo,^{11,12} F. Loparco,^{23,24} B. Lott,^{37,38} M. N. Lovellette,¹ P. Lubrano,^{21,22} G. M. Madejski,² A. Makeev,¹²⁹ B. Marangelli,^{23,24} M. N. Mazziotta,²⁴ S. McBreen,^{19,48} J. E. McEnery,¹⁰ S. McGlynn,^{5,16} C. Meegan,⁴⁰ P. Mészáros,²⁶ C. Meurer,^{5,32} P. F. Michelson,² M. Minuti,⁷ N. Mirizzi,^{23,24} W. Mitthumsiri,² T. Mizuno,⁴¹ A. A. Moiseev,⁹ C. Monte,^{23,24} M. E. Monzani,² E. Moretti,^{11,12} A. Morselli,⁴⁹ I. V. Moskalenko,² S. Murgia,² T. Nakamori,³ D. Nelson,² P. L. Nolan,² J. P. Norris,⁵⁰ E. Nuss,³⁰ M. Ohno,⁵¹ T. Ohsugi,⁴¹ A. Okumura,⁵² N. Omodei,⁷ E. Orlando,¹⁹ J. F. Ormes,⁵⁰ M. Ozaki,⁵¹ W. S. Paciesas,¹⁸ D. Paneque,² J. H. Panetta,² D. Parent,^{37,38} V. Pelassa,³⁰ M. Pepe,^{21,22} M. Perri,³³ M. Pesce-Rollins,⁷ V. Petrosian,^{23,24} M. Pinchera,⁷ F. Pirion,³⁰ T. A. Porter,⁴ R. Preece,⁴⁰ S. Rainò,^{23,24} E. Ramirez-Ruiz,⁵³ R. Rando,^{14,15} E. Rapposelli,⁷ M. Razzano,⁷ S. Razzaque,¹ N. Rea,⁵⁴ A. Reimer,² O. Reimer,² T. Reposeur,^{37,38} L. C. Reyes,⁵⁵ S. Ritz,^{9,42} L. S. Rochester,² A. Y. Rodriguez,⁵⁴ M. Roth,²⁵ F. Ryde,^{5,16} H. F.-W. Sadrozinski,⁴ D. Sanchez,²⁰ A. Sander,¹⁷ P. M. Saz Parkinson,⁴ J. D. Scargle,⁵⁶ T. L. Schalk,⁴ K. N. Segal,⁹ C. Sgrò,⁷ T. Shimokawabe,³ E. J. Siskind,⁵⁷ D. A. Smith,^{37,38} P. D. Smith,¹⁷ G. Spandre,⁷ P. Spinelli,^{23,24} M. Stamatikos,¹⁰ J.-L. Starck,⁸ F. W. Stecker,¹⁰ H. Steinkle,¹⁹ T. E. Stephens,¹⁰ M. S. Strickman,¹ D. J. Suson,⁵⁸ G. Tagliaferri,⁵⁹ H. Tajima,²⁴ H. Takahashi,⁴¹ T. Takahashi,⁵¹ T. Tanaka,⁴ A. Tenze,⁷ J. B. Thayer,² J. G. Thayer,² J. Thompson,¹⁰ L. Tibaldo,^{14,15} D. F. Torres,^{54,60} G. Tosti,^{21,22} A. Tramacere,^{2,61} M. Turri,² S. Tuvi,²

T. L. Usher,² A. J. van der Horst,⁴⁰ L. Vigiani,⁷ N. Vilchez,⁴⁶ V. Vitale,^{49,62} A. von Kienlin,¹⁹ A. P. Waite,² D. A. Williams,⁴ C. Wilson-Hodge,⁴⁰ B. L. Winer,¹⁷ K. S. Wood,¹ X. F. Wu,^{26,63,64} R. Yamazaki,⁴¹ T. Ytinen,^{5,16,65} M. Ziegler⁴

¹Space Science Division, Naval Research Laboratory, Washington, DC 20375, USA. ²W. W. Hansen Experimental Physics Laboratory, Kavli Institute for Particle Astrophysics and Cosmology, Department of Physics and SLAC National Accelerator Laboratory, Stanford University, Stanford, CA 94305, USA. ³Department of Physics, Tokyo Institute of Technology, Meguro City, Tokyo 152-8551, Japan. ⁴Santa Cruz Institute for Particle Physics, Department of Physics, and Department of Astronomy and Astrophysics, University of California at Santa Cruz, Santa Cruz, CA 95064, USA. ⁵The Oskar Klein Centre for Cosmo Particle Physics, AlbaNova, SE-106 91 Stockholm, Sweden. ⁶Department of Astronomy, Stockholm University, SE-106 91 Stockholm, Sweden. ⁷Istituto Nazionale di Fisica Nucleare, Sezione di Pisa, I-56127 Pisa, Italy. ⁸Laboratoire AIM, CEA-IRFU/CNRS/Université Paris Diderot, Service d'Astrophysique, CEA Saclay, 91191 Gif sur Yvette, France. ⁹Center for Research and Exploration in Space Science and Technology (CRESTT), NASA Goddard Space Flight Center, Greenbelt, MD 20771, USA. ¹⁰National Aeronautics and Space Administration (NASA) Goddard Space Flight Center, Greenbelt, MD 20771, USA. ¹¹Istituto Nazionale di Fisica Nucleare, Sezione di Trieste, I-34127 Trieste, Italy. ¹²Dipartimento di Fisica, Università di Trieste, I-34127 Trieste, Italy. ¹³Department of Physics and Astronomy, Rice University, MS-108, Post Office Box 1892, Houston, TX 77251, USA. ¹⁴Istituto Nazionale di Fisica Nucleare, Sezione di Padova, I-35131 Padova, Italy. ¹⁵Dipartimento di Fisica "G. Galilei," Università di Padova, I-35131 Padova, Italy. ¹⁶Department of Physics, Royal Institute of Technology (KTH), AlbaNova, SE-106 91 Stockholm, Sweden. ¹⁷Department of Physics, Center for Cosmology and Astro-Particle Physics, The Ohio State University, Columbus, OH 43210, USA. ¹⁸University of Alabama in Huntsville, Huntsville, AL 35899, USA. ¹⁹Max-Planck Institut für Extraterrestrische Physik, 85748 Garching, Germany. ²⁰Laboratoire Leprince-Ringuet, Ecole Polytechnique, CNRS/IN2P3, Palaiseau, France. ²¹Istituto Nazionale di Fisica Nucleare, Sezione di Perugia, I-06123 Perugia, Italy. ²²Dipartimento di Fisica, Università degli

Studi di Perugia, I-06123 Perugia, Italy. ²³Dipartimento di Fisica "M. Merlin," dell'Università e del Politecnico di Bari, I-70126 Bari, Italy. ²⁴Istituto Nazionale di Fisica Nucleare, Sezione di Bari, 70126 Bari, Italy. ²⁵Department of Physics, University of Washington, Seattle, WA 98195-1560, USA. ²⁶Pennsylvania State University, 525 Davey Laboratory, University Park, PA 16802, USA. ²⁷INAF (Istituto di Astrofisica Spaziale e Fisica Cosmica), I-20133 Milano, Italy. ²⁸Scuola Internazionale Superiore di Studi Avanzati (SISSA), 34014 Trieste, Italy. ²⁹George Mason University, Fairfax, VA 22030, USA. ³⁰Laboratoire de Physique Théorique et Astroparticules, Université Montpellier 2, CNRS/IN2P3, 34095 Montpellier, France. ³¹Department of Physics and Astronomy, Sonoma State University, Rohnert Park, CA 94928-3609, USA. ³²Department of Physics, Stockholm University, AlbaNova, SE-106 91 Stockholm, Sweden. ³³Agenzia Spaziale Italiana (ASI) Science Data Center, I-00044 Frascati (Roma), Italy. ³⁴Stellar Solutions Incorporated, 250 Cambridge Avenue, Suite 204, Palo Alto, CA 94306, USA. ³⁵Dipartimento di Fisica, Università di Udine and Istituto Nazionale di Fisica Nucleare, Sezione di Trieste, Gruppo Collegato di Udine, I-33100 Udine, Italy. ³⁶Los Alamos National Laboratory, Los Alamos, NM 87545, USA. ³⁷CNRS/IN2P3, Centre d'Études Nucléaires Bordeaux Gradignan, UMR 5797, Gradignan, 33175, France. ³⁸Université de Bordeaux, Centre d'Études Nucléaires Bordeaux Gradignan, UMR 5797, Gradignan, 33175, France. ³⁹Department of Physics and Astronomy, University of Leicester, Leicester, LE1 7RH, UK. ⁴⁰NASA Marshall Space Flight Center, Huntsville, AL 35805, USA. ⁴¹Department of Physical Science and Hiroshima Astrophysical Science Center, Hiroshima University, Higashi-Hiroshima 739-8526, Japan. ⁴²University of Maryland, College Park, MD 20742, USA. ⁴³Centre for Astrophysics Research, University of Hertfordshire, College Lane, Hatfield AL10 9AB, UK. ⁴⁴European Organization for Nuclear Research (CERN), CH-1211 Geneva, Switzerland. ⁴⁵Cosmic Radiation Laboratory, Institute of Physical and Chemical Research (RIKEN), Wako, Saitama 351-0198, Japan. ⁴⁶Centre d'Étude Spatiale des Rayonnements, CNRS/UPS, BP 44364, F-30128 Toulouse Cedex 4, France. ⁴⁷Orbital Network Engineering, 10670 North Tantau Avenue, Cupertino, CA 95014, USA. ⁴⁸University College Dublin, Belfield, Dublin 4, Ireland. ⁴⁹Istituto Nazionale di Fisica Nucleare, Sezione di Roma "Tor Vergata," I-00133 Roma, Italy. ⁵⁰Department of Physics

and Astronomy, University of Denver, Denver, CO 80208, USA. ⁵¹Institute of Space and Astronautical Science, Japan Aerospace Exploration Agency (JAXA), 3-1-1 Yoshinodai, Sagami-hara, Kanagawa 229-8510, Japan. ⁵²Department of Physics, Graduate School of Science, University of Tokyo, 7-3-1 Hongo, Bunkyo-ku, Tokyo 113-0033, Japan. ⁵³University of California Observatories/Lick Observatories, Santa Cruz, CA 95064, USA. ⁵⁴Institut de Ciències de l'Espai (IEEC-CSIC), Campus UAB, 08193 Barcelona, Spain. ⁵⁵Kavli Institute for Cosmological Physics, University of Chicago, Chicago, IL 60637, USA. ⁵⁶Space Sciences Division, NASA Ames Research Center, Moffett Field, CA 94035-1000, USA. ⁵⁷NYCB Real-Time Computing Incorporated, Lattingtown, NY 11560-1025, USA. ⁵⁸Department of Chemistry and Physics, Purdue University Calumet, Hammond, IN 46323-2094, USA. ⁵⁹INAF Osservatorio Astronomico di Brera, I-23807 Merate, Italy. ⁶⁰Institució Catalana de Recerca i Estudis Avançats (ICREA), 08010 Barcelona, Spain. ⁶¹Consorzio Interuniversitario per la Fisica Spaziale (CIFS), I-10133 Torino, Italy. ⁶²Dipartimento di Fisica, Università di Roma "Tor Vergata," I-00133 Roma, Italy. ⁶³Joint Center for Particle Nuclear Physics and Cosmology (J-CNPCC), Nanjing 210093, China. ⁶⁴Purple Mountain Observatory, Chinese Academy of Sciences, Nanjing 210008, China. ⁶⁵School of Pure and Applied Natural Sciences, University of Kalmar, SE-391 82 Kalmar, Sweden.

*To whom correspondence should be addressed. E-mail: michael.briggs@nasa.gov (M.S.B.); htajima@slac.stanford.edu (H.T.); charles.dermer@nrl.navy.mil (C.D.D.).

†Present address: Sterrenkundig Instituut "Anton Pannekoek," 1098 SJ Amsterdam, Netherlands.

Supporting Online Material

www.sciencemag.org/cgi/content/full/1169101/DC1

SOM Text

Figs. S1 to S7

Movie S1

27 November 2008; accepted 11 February 2009

Published online 19 February 2009;

10.1126/science.1169101

Include this information when citing this paper.

Comprehensive Characterization of Genes Required for Protein Folding in the Endoplasmic Reticulum

Martin C. Jonikas,^{1,2,3,4} Sean R. Collins,^{1,3,4} Vladimir Denic,^{1,3,4*} Eugene Oh,^{1,3,4} Erin M. Quan,^{1,3,4} Volker Schmid,⁵ Jimena Weibezahn,^{1,3,4} Blanche Schwappach,⁵ Peter Walter,^{2,3} Jonathan S. Weissman,^{1,3,4,†} Maya Schuldiner^{1,3,4,‡}

Protein folding in the endoplasmic reticulum is a complex process whose malfunction is implicated in disease and aging. By using the cell's endogenous sensor (the unfolded protein response), we identified several hundred yeast genes with roles in endoplasmic reticulum folding and systematically characterized their functional interdependencies by measuring unfolded protein response levels in double mutants. This strategy revealed multiple conserved factors critical for endoplasmic reticulum folding, including an intimate dependence on the later secretory pathway, a previously uncharacterized six-protein transmembrane complex, and a co-chaperone complex that delivers tail-anchored proteins to their membrane insertion machinery. The use of a quantitative reporter in a comprehensive screen followed by systematic analysis of genetic dependencies should be broadly applicable to functional dissection of complex cellular processes from yeast to human.

The endoplasmic reticulum (ER) is responsible for the folding and maturation of secreted and membrane proteins. External stress or mutations can compromise ER folding, contributing to diseases such as diabetes and neurodegeneration (1, 2). The specialized milieu of the ER is composed of a large number of proteins that aid the structural maturation of itinerant proteins (3, 4). Although many of these ER folding factors

have been extensively studied, the full range of proteins contributing to this process is unknown, and how they function together is poorly understood.

Systematic identification of genes contributing to ER folding. We exploited the cell's endogenous sensor of ER protein folding status, Ire1p, to identify genes in *Saccharomyces cerevisiae* that contribute to structural maturation of secretory proteins. In response to misfolded proteins in

the ER, the transmembrane sensor Ire1p activates the transcription factor Hac1p (5), which in turn transcriptionally up-regulates a distinct set of genes (6, 7) in a process called the unfolded protein response (UPR). We used a reporter system in which a Hac1p-responsive promoter drives green fluorescent protein (GFP) expression (8) (Fig. 1A). To correct for nonspecific expression changes, we coexpressed a red fluorescent protein (RFP) from a constitutive *TEF2* promoter and used the ratio of GFP/RFP as our reporter of UPR signaling. A titration of the ER stress-inducing reducing agent dithiothreitol (DTT) demonstrated that this reporter quantitatively responds to misfolding of ER proteins (Fig. 1B).

With use of synthetic genetic array methodology (9), we introduced the reporter into ~4500 strains from the *S. cerevisiae* deletion library (10),

¹Department of Cellular and Molecular Pharmacology, University of California, San Francisco, San Francisco, CA 94143, USA. ²Department of Biochemistry and Biophysics, University of California, San Francisco, San Francisco, CA 94143, USA. ³Howard Hughes Medical Institute, University of California, San Francisco, San Francisco, CA 94143, USA. ⁴California Institute for Quantitative Biomedical Research, San Francisco, CA 94143, USA. ⁵Faculty of Life Sciences, University of Manchester, Manchester M13 9PT, UK.

*Present address: Department of Molecular and Cellular Biology, Harvard University, Cambridge, MA 02138, USA.

†To whom correspondence should be addressed. E-mail: weissman@cmp.ucsf.edu

‡Present address: Department of Molecular Genetics, Weizmann Institute of Science, Rehovot 76100, Israel.